Journal of Porous Materials (2023) 30:1459–1468
https://doi.org/10.1007/s10934-023-01433-3

# The effect of amorphous silica support on the catalytic activity of liquid-exfoliated monolayered MCM-56 zeolite

**Karolina Ogorzały[1] · Gabriela Jajko[1,2] · Aleksandra Korzeniowska[1] · Michal Mazur[3] · Ang Li[3] · Wieslaw J. Roth[1] · Barbara Gil[1] · Wacław Makowski[1]**

Accepted: 9 February 2023 / Published online: 2 March 2023


**Abstract**
Recently reported groundbreaking discovery of efficient delamination of zeolite MCM-56, producing colloidal suspensions of MWW monolayers dispersed in the liquid phase, created unprecedented possibilities for the synthesis of a zeolite catalyst. Based on this innovation, the concept of using MWW monolayers to prepare silica-supported zeolite nanosheet catalysts suitable for transformations of large organic molecules was explored in this work. A series of silica-MWW preparations was synthesized from colloidal suspensions of the monolayers, using both solid and colloidal silica sources. The synthesized solids were thoroughly characterized with various physicochemical methods and their catalytic performance was tested in alkylation of mesitylene with benzyl alcohol. The obtained results indicate that solids containing MWW layers dispersed on silica show promising catalytic properties. The mixed MWW:silica catalysts synthesized from dispersions of MWW monolayers and liquid silica were found to exhibit high specific catalytic activity (with TOF values of $3.4\times10^{-3}$ to $4.8\times10^{-3}$ $s^{-1}$), despite the high content of inactive amorphous silica support (40–60%). Materials synthesized from solid fumed and precipitated silicas showed low or negligible overall activity, which could be attributed to the small incorporation of the zeolitic active phase. For one of such materials, a notable high TOF ($4.8\times10^{-3}$ $s^{-1}$) was found. It was found earlier that ethanol is an effective flocculent for zeolite layers by themselves, but in the presence of solid silica its efficiency was reduced.

**Keywords** Layered zeolites · MCM-56 · MWW colloids · Exfoliation · Catalysis · Friedel-Crafts alkylation

## 1 Introduction

The growth of industries has resulted in large-scale production of goods and consumption, which induced a considerable rise in the standard of living, but it also presents a substantial threat to human health and the environment [1–6]. The importance of heterogeneous catalysis cannot be overestimated in both areas, since it is assessed that 90% of chemical technology processes utilize heterogeneous catalysts [7–9]. Porous materials, especially microporous zeolites, constitute an important class of heterogeneous catalysts [10–12]. However, modern catalysts must offer not only high surface areas and superior acidity but also mesopores or hierarchical pore structures to enhance diffusion and hence activity in the conversion of large organic molecules [13–15].

Post-synthesis treatment of classic 3D zeolites, originally limited to ion-exchange or isomorphic substitutions, was successfully followed by dealumination or desilication, leading to a change in the porosity due to partial structure modification [16]. The discovery of layered precursors of zeolites, was a game changer because pore enlargement beyond the 1 nm limit and enhancement of the external surface areas could since then be realized by non-destructive methods, preserving the layer integrity—via swelling, delamination, pillaring, or silylation [17–23]. The availability of exfoliated zeolite monolayers [24], suspended in a solution, allowed another breakthrough—combination with any particle, layer

✉ Barbara Gil
barbara.k.gil@uj.edu.pl

✉ Wacław Makowski
waclaw.makowski@uj.edu.pl

[1] Faculty of Chemistry, Jagiellonian University, Gronostajowa 2, 30-387 Kraków, Poland

[2] Doctoral School of Exact and Natural Sciences, Jagiellonian University, Łojasiewicza 11, Kraków 30-348, Poland

[3] Department of Physical and Macromolecular Chemistry, Faculty of Science, Charles University, Hlavova 8, 12840 Prague 2, Czech Republic

or reagent to produce nanoscale composite and hierarchical materials, exemplified by zeolite–zeolite intimate structures [25], and in the future also with other two-dimensional crystals obtained via delamination/exfoliation [26, 27]. Previously studied systems included MWW layers with siliceous MFI and showed that dilution of the former active phase with the latter up to 50% did not reduce the overall activity. This presents a question about the behavior of intimate hybrids comprising zeolite monolayers and inert silica, the latter acting as a support and skeletal reinforcement or binder in the formed catalyst. In our previous work, MWW monolayers were precipitated by an ethanoic solution of tetraethyl *ortho*silicate (TEOS) in the presence of isopropyl alcohol to produce pillared MWW derivatives [28]. The possibility investigated here, is based on the deposition of MWW layers on the solid silica, or co-precipitation of $SiO_2$ with MWW layers, to produce a supported zeolite catalyst. Different types of silica are examined: Aerosil A200 (fumed silica, Evonic), Ultrasil VN3 (precipitated silica, Grolman), and Ludox LS (colloidal silica, Sigma Aldrich, LS-30).

## 2 Experimental

### 2.1 MCM-56 synthesis and preparation of monolayer dispersions

The parent MCM-56 zeolite was prepared, using the published procedures [29–31], from the following reagents: deionized water, 50% NaOH solution (Sigma Aldrich), sodium aluminate (Riedel-de Haën, 40–45% $Na_2O$, 50–-56% $Al_2O_3$), hexamethyleneimine (HMI, 99%, Sigma Aldrich), aniline (AN, > 99%, Sigma Aldrich), and Aerosil (A200, Evonic) in the following molar ratios: Si/Al = 12.5, OH/Si = 0.18, HMI/Si = 0.1, AN/Si = 0.2 and $H_2O$/Si = 45. The reaction mixture was placed in a Teflon-lined autoclave, rotated overnight at room temperature, and then heated at 143 °C for 176 h. The solid was isolated by filtration, washed with deionized water, and dried at room temperature. The sample was denoted as MWW_parent.

Colloidal dispersions of unilamellar MWW nanosheets were prepared using the published procedure [24]. 0.4 g of MCM-56 (MWW parent) was mixed with 5.9 g 40% tetrabutylammonium hydroxide (TBAOH) and 14.8 g of deionized water and stirred for 2 h at room temperature, followed by centrifugation at 10,000 rpm (10K rpm) for 30 min and decantation of the supernatant as a discard. The remaining wet solid was stirred with 20 ml of water for another 2 h, centrifuged for 30 min at 10K rpm, and decanted as a translucent liquid. Typically, 0.4 g of MCM-56 yielded 0.2 g of precipitated MWW nanosheets and 0.15 g when calcined. The sample was denoted MWW_coll.

### 2.2 Preparation of silica-supported zeolite catalysts

Three different MWW:silica mixtures were prepared using Aerosil (Aerosil A200, Evonic), Ultrasil (VN3, Grolman), and Ludox (LS30, Sigma Aldrich, 30%wt solution) as a fumed, precipitated and colloidal silica sources, respectively. The starting weight ratio of MWW to silica was fixed to 1:1. The samples were denoted MWW:1Aerosil, MWW:1Ultrasil, MWW:1Ludox. Additional formulations were obtained using a twofold and threefold excess of silica for the most promising catalysts: MWW:2Aerosil, MWW:2Ludox, MWW:3Ludox. The mixtures of silica and MWW colloid were stirred overnight at room temperature. After that, 45 ml of ethyl alcohol was added as the precipitating agent. The resulting solids were centrifuged and washed with deionized water. The final materials were obtained by calcination at 540 °C for 6 h in air. The yields observed in these syntheses differed considerably, from only 2–4% for the materials obtained using Ludox as a silica source to 29–51% for those based on the solid silicas. Additionally, the reference material, MWW:Ludox_p, was prepared, the physical mixture of precipitated MWW layers (MWW_coll) with dried Ludox, with a 1:1 ratio.

### 2.3 Material characterization

The crystallinity of the obtained materials was determined by powder X-ray diffraction, using a Rigaku MiniFlex diffractometer in refection mode with Cu-Kα radiation (λ = 0.154 nm) in the ranges 3°–30° 2θ. The XRD patterns were collected with steps of 0.02°.

Scanning transmission electron microscopy (STEM) imaging was carried out to assess the morphology and distribution of the MCM-56 layers using a JEOL NeoARM 200F microscope operated at 200 kV. Images were collected using annular dark-field (ADF) and annular bright-field (ABF) detectors. The alignment of the microscope was performed using the standard Ronchigram adjustment method.

The concentrations of Lewis (LAS) and Brønsted (BAS) acid sites were determined using pyridine adsorption [32], followed by IR spectroscopy (Tensor 27 from Bruker, MTC detector, spectral resolution 2 $cm^{-1}$). The following absorption coefficients were used: ε(Py-LAS) = 0.165 $cm^2$/μmol, and ε(Py-BAS) = 0.044 $cm^2$/μmol. The calcined zeolites were pressed into self-supporting wafers and activated in situ at 500 °C for 1 h at vacuum ($10^{-3}$ mbar) in a home-made quartz cell, allowing activation and adsorption inside the infrared spectrometer. After adsorption of the pyridine vapor at 170 °C (ca. 20 mbar equilibrium pressure), the samples were evacuated for 20 min and the spectrum was collected. All spectra were recalculated to the same mass equal to 10 mg.

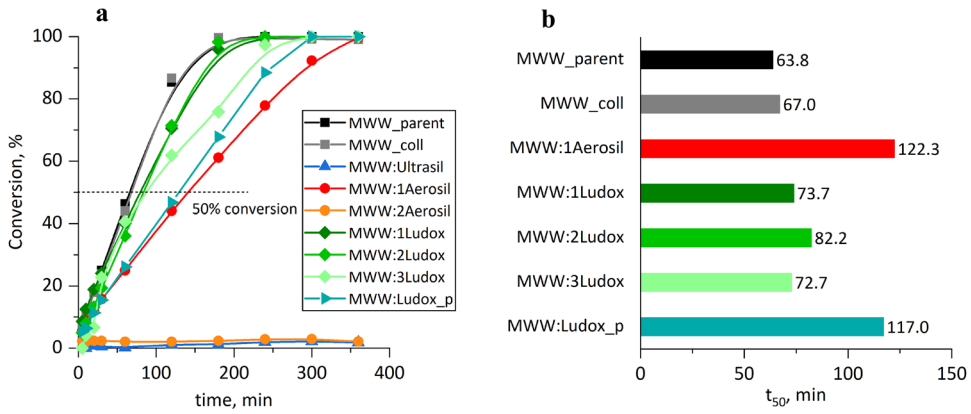


**Fig. 1** **a** The conversion of benzyl alcohol (at 80 °C) vs. time for the tested materials, and **b** time of 50% ($t_{50}$) of benzyl alcohol

Nitrogen adsorption/desorption isotherms at − 196 °C (liquid nitrogen temperature) were determined using a static volumetric Autosorb IQ apparatus (Quantachrome Instruments). Prior to the measurements, all samples were activated under vacuum for 0.5 h at 80 °C, 0.5 h at 120 °C, and 8 h at 350 °C (2 °C/min). Specific surface area values were determined using the BET method. The mesopore and external surface area values, micro- and mesopore volumes were obtained using the t-plot method. Pore size distributions were calculated based on $N_2$ adsorption data using the NLDFT model provided by ASiQwin (Quantachrome) software for zeolite/silica with cylindrical pores.

Porosity was additionally studied by quasi-equilibrated temperature programmed desorption and adsorption (QE-TPDA) of hexane. A detailed description of the experimental procedures has been described in our previous works [33–35]. Prior to the QE-TPDA measurements, a sample (ca. 6 mg) placed in a quartz tube was activated by heating to 500 °C (10 °C/min) in the flow of helium (7.3 $cm^3$/min), then it was cooled to room temperature. After the activation, the hexane vapor was added to the helium stream resulting in isothermal sorption at room temperature. The thermal conductivity detector signal, consisting of desorption maxima and adsorption minima, recorded while the sample was cyclically heated and cooled at a constant rate of 5 °C/min, represented a QE-TPDA profile.

### 2.4 Catalytic tests

The catalytic test reaction, liquid phase alkylation of mesitylene with benzyl alcohol, was carried out in a two-neck round-bottom flask (equipped with a reflux condenser) heated in a multi-experiment workstation StarFish (Radleys Discovery Technologies) under atmospheric pressure. The reaction temperature was 80 °C. Prior to the reaction, the calcined solids were ion-exchanged into $NH_4^+$ form, with a 1 M solution of $NH_4NO_3$ (three times, 20 ml, 1 h at room temperature), washed with deionized water, dried, and activated at 500 °C for 5 h to obtain active hydrogen forms with minimized content of metal cations such as sodium. Aliquots of 22 ml of mesitylene, 50 mg of the studied catalyst, and 0.1 g of dodecane, as an internal standard, were combined. The reaction mixture was maintained for 30 min at 80 °C and then 0.2 g of benzyl alcohol was added. This moment was considered as the beginning of the reaction. The liquid samples were withdrawn at regular intervals and analysed by the PerkinElmer Clarus 600 GC gas chromatograph with an FID detector using a 30 m column Elite-1MS. The amount of reaction liquid to be dosed was 1 µl. The column temperature program was as follows: 90 °C for 6 min, then heating to 300 °C, ramp 20 °C/min and hold for 0.5 min. The diameter of the internal column was 0.35 mm.

The conversion of benzyl alcohol was calculated using the following equation.

$$\alpha = k\frac{A_{Bz}}{A_{IS} \cdot n_0}100\%,$$

where k is calibration factor (1.13 mol), $A_x$ is area of the peak on the chromatogram for benzyl alcohol ($A_{Bz}$) or internal standard ($A_{IS}$), $n_0$ is initial amount of benzyl alcohol (mol).

## 3 Results and discussion

The most important property of the MWW:silica mixtures is their catalytic activity, expressed here as $t_{50}$, that is, the time to achieve 50% conversion of benzyl alcohol in its reaction with mesitylene (Fig. 1a, b; Table 1). The higher the activity, the lower the $t_{50}$ values. We used Friedel–Crafts alkylation of mesitylene by benzyl alcohol as the test reaction, because it is well understood and used to gauge the accessibility of larger molecules for zeolites from the MWW family like MCM-22, MCM-49 and MCM-56 [36–38], as well as their swollen and pillared derivatives [30, 39]. Mesitylene cannot access the 10-rings of MWW zeolite, therefore the reaction is primarily occurring on the external surfaces of the

**Table 1** Physicochemical properties of the studied zeolites: textural parameters calculated from $N_2$ adsorption isotherms (a) and QE-TPDA profiles of hexane (b); BAS and LAS concentrations calculated using pyridine as a probe molecule for FTIR studies; $t_{50}$ values correspond to the 50% conversion time of benzyl alcohol in Friedel–Crafts alkylation with mesitylene at 80 °C

| Sample | $S_{BET}$ ($m^2$/g) | $V_{micro}$[a] ($cm^3$/g) | $V_{micro}$[b] ($cm^3$/g) | BAS (μmol/g) | LAS (μmol/g) | $t_{50}$ (min) | TOF ($10^{-3}$ $s^{-1}$) | MWW (%) |
|---|---|---|---|---|---|---|---|---|
| MWW_parent | 399 | 0.07 | 0.10 | 892 | 91 | 64 | 2.9 | 100 |
| MWW_coll | 452 | 0.11 | 0.11 | 949 | 245 | 67 | 2.4 | 98 |
| MWW:Ultrasil | 187 | 0.01 | 0.02 | 107 | 11 | – | | 8 |
| MWW:1Aerosil | 205 | 0.00 | 0.05 | 335 | 86 | 122 | 4.8 | 20 |
| MWW:2Aerosil | 153 | 0.01 | 0.01 | 0 | 381 | – | | 1 |
| MWW:1Ludox | 272 | 0.00 | 0.07 | 628 | 167 | 74 | 4.1 | 56 |
| MWW:2Ludox | 265 | 0.01 | – | 607 | 91 | 82 | 3.4 | 50 |
| MWW:3Ludox | 203 | 0.00 | 0.08 | 471 | 95 | 73 | 4.8 | 43 |
| MWW:Ludox_p | 351 | 0.01 | 0.07 | – | – | 117 | | 28 |
| Ultrasil | 202 | 0.01 | – | – | – | – | | – |
| Aerosil | 225 | 0.00 | – | – | – | – | | – |
| Ludox | 263 | 0.00 | – | – | – | – | | – |

The relative content of MWW was calculated on the basis of the integral intensities of double six ring (D6R) FT-IR maxima (see text for details). Ludox refers to the solid sample precipitated by $NH_4NO_3$. TOF values were calculated on the basis of BAS concentration and $t_{50}$ values

layers (in the external cups and pore mouths). Remarkably, even when the zeolite content was reduced due to the presence of chemically and catalytically inactive silica, the $t_{50}$ values were only slightly higher for MWW deposited on silicas, especially for MWW:1Ludox samples (73–82 min), in comparison to the pure phases: the parent MWW (64 min) and precipitated monolayers—MWW_coll (67 min). The MWW:1Ultrasil sample was not active even with the 1:1 MWW:silica ratio and the activity of the MWW:1Aerosil was quite low ($t_{50}$ = 122 min) and become negligible for MWW:2Aerosil.

Samples may be assigned to three groups: one with high activity (MWW_parent, MWW_coll, together with MWW:1Ludox and MWW:2Ludox), second with very low activity (MWW:2 Aerosil, MWW:Ultrasil), and the third with intermediate activity (MWW:1Aerosil, MWW:3Ludox, MWW:Ludox_p). The use of liquid phase silica (Ludox) decreased the activity only slightly despite a reduction of the zeolite phase content by about one-half. This is similar to the composite of MWW layers with siliceous MFI (catalytic activity was comparable to the parent material while the MWW content was diluted by 50%; for a physical mixture of MCM-56 and MFI, the activity decreased by half) [25]. When pillared zeolites were produced from exfoliated MWW monolayers in solution, the reaction was faster than for the parent sample [28].

The quality of the tested MWW materials was first assessed by powder XRD (Fig. 2). The XRD patterns contained reflections characteristic for MWW zeolites at 7.2° 2θ (hkl 100), ca. 25 and 26° 2θ (220, 310) as well as a wide peak between 8° and 10° 2θ (related to 101 and 102), without the dip indicating spatially disorganized layers [30, 40, 41]. The quality of the parent MWW and the layers precipitated from the colloid (MWW_coll) seem to be comparable,

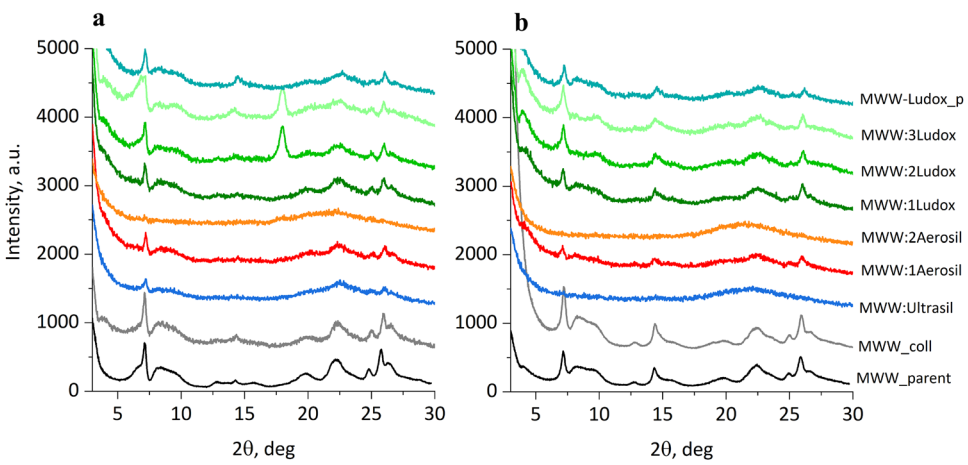


**Fig. 2** XRD patterns of uncalcined (**a**) and calcined (**b**) MWW samples

as indicated by a similar overall intensity of the XRD pattern and absent valley at 8°–10° 2θ as evidence of disordered layers. The materials obtained with solid silicas, Ultrasil and Aerosil, seem to be practically amorphous with very weak reflections due to MWW that disappear almost completely after calcination. In contrast, precipitation of the MWW colloid nanosheets in the presence of the liquid silica source, Ludox, resulted in samples with clearly present crystalline phase. It should be noted that with increasing concentration of silica the intensity of scattering near 10° 2θ becomes elevate creating impressing of a dip between 8° and 10° 2θ, which might imply ordering of the layers. The effect is minor and may be caused by other factors, so for now it must be considered unknown. This scattering has a triangular shape that resembles the XRD of SSZ-70 [42, 43] but its position and the presence of scattering around 8° 2θ rule out this possibility. The intense reflections at ca. 18° 2θ for MWW:2Ludox and MWW:3Ludox, are probably due to the presence of organics (TBAOH), because they disappear after calcination. In conclusion, the use of liquid silica source (Ludox) seems to be the most advantageous for the formation of the MWW:silica composites, ensuring incorporation of the zeolite layers. At the same time, the model catalytic activity is also the highest for all MWW:Ludox samples, almost independently of the MWW content. Even the sample with the lowest MWW content (MWW:3Ludox) performs better than the samples made with the use of solid silicas, for which the MWW content is higher.

Nitrogen adsorption together with QE-TPDA was used as a complementary tool for assessing the properties of the products. The nitrogen adsorption–desorption isotherms for the studied materials are presented in Fig. 3. Although in the case of Aerosil and Ultrasil the isotherms are typical for nonporous materials, the one observed for Ludox-based silica reveals the presence of mesopores (Fig. 3a). The triangular hysteresis loop (type H2a), related to the capillary condensation, with nearly vertical closing, should be attributed to the interconnected, partially restricted mesopore system [44]. Similar adsorption–desorption hysteresis loops have been observed for ordered mesoporous silicas SBA-16 and KIT-5, containing large spherical pores interconnected with much smaller windows [45]. The shape of the isotherm observed for pure MWW materials (Fig. 3b). is characteristic of microporous solids with a considerable content of large, usually intercrystalline, mesopores [46]. In the isotherms obtained for the MWW:silica materials, smaller offsets in the low-pressure range may be observed than in those observed for the pristine MWW materials, indicating smaller micropore volumes. Indeed, the t-plot analysis of these isotherms resulted in low values of the micropore volume. However, we have previously found [28] that this method can underestimate micropore volume in modified

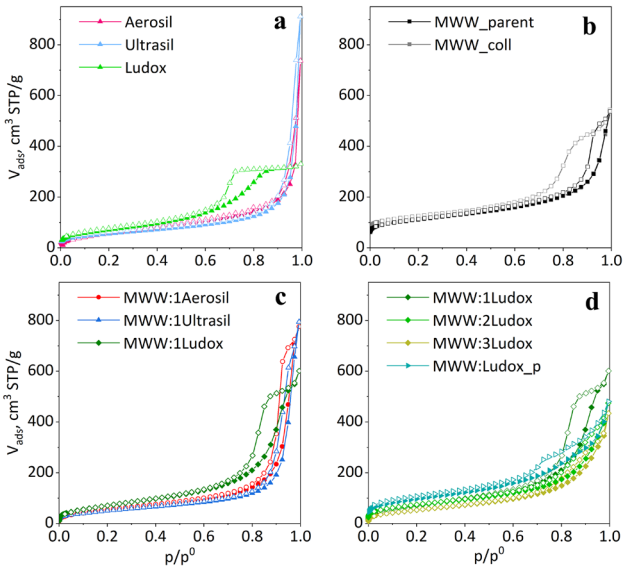


**Fig. 3** $N_2$ adsorption–desorption isotherms of the studied samples. Closed symbols stand for adsorption and open symbols stand for desorption

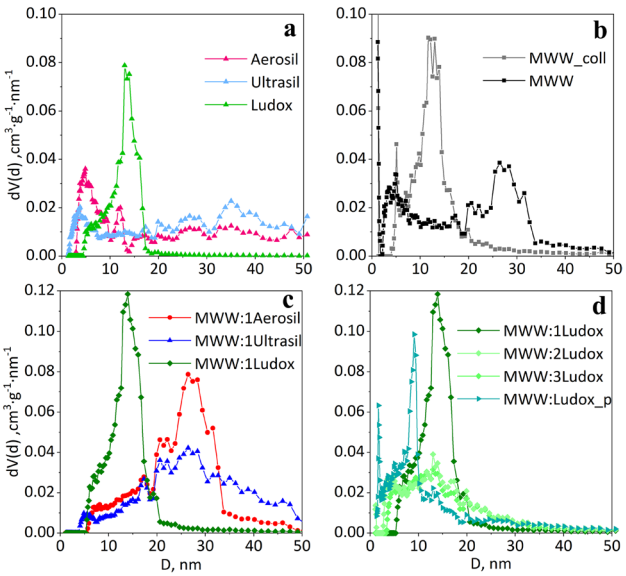


**Fig. 4** Pore size distributions calculated using the NLDFT method (equilibrium model)

MWW zeolites and a more realistic picture is obtained with QE-TPDA, as discussed later.

The pore size distributions (Fig. 4), calculated from $N_2$ desorption isotherms using the NLDFT method, show more precisely differences in the porosity of the studied materials. Among pure silica samples, only Ludox shows the presence of mesopores with a characteristic prominent peak between 10 and 20 nm with the maximum at about 13 nm. Both the MWW layers alone from colloid and all MWW:Ludox

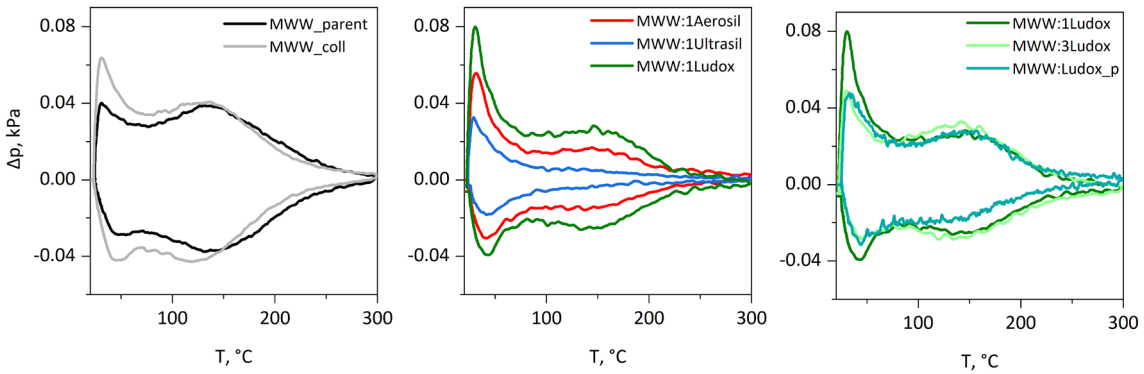


**Fig. 5** QE-TPDA profiles for hexane sorption (5 °C/min)

preparations show a similar mesopore size distribution, most uniform in the 1:1 sample. In contrast, the calcined parent zeolite (MWW_parent) contains mainly larger mesopores (25–30 nm). It is more likely that the mesoporosity observed with the MWW:Ludox mixtures has more to do with the former (the arrangement of the zeolite layers) than with the Ludox component. This conclusion is postulated because the intensity of the PSD peak decreases with increasing Ludox content. Aerosil- and Ultrasil-based MWW:silica materials have much larger mesopores (20–35 nm) than those of the Ludox counterpart. The mesopores in all prepared MWW:silica materials are large enough to accommodate the reactants of the Friedel–Crafts reaction; hence, their actual size has in all probability a negligible effect on the catalytic activity of the materials.

The high intensity of the PSDs for both MWW zeolites alone at very low pore size values indicates considerable microporosity of these materials, the micropore volumes are 0.07 and 0.11 $cm^3/g$ for MWW_parent and MWW_coll, respectively. All MWW:silica samples have low microporosity, very hard to characterize properly by low temperature nitrogen adsorption.

As mentioned earlier, values of the micropore volume determined from $N_2$ adsorption isotherms using the t-plot method are often underestimated. For this reason, we applied QE-TPDA of hexane as an additional method for assessing microporosity of the studied materials. Due to the low relative pressure of the adsorptive in the carrier gas, applied in these measurements ($p/p_s \approx 0.03$), initial adsorption in these experiments is limited to the micropores. The QE-TPDA profiles shown in Fig. 5 exhibit broad desorption maxima and adsorption maxima, corresponding to structural MWW micropores. They confirm the microporosity of the studied MWW:silica materials, except for MWW:1Ultrasil and MWW:2Aerosil. Additional low-temperature maxima (in the 25–50 °C range) should be attributed to the strongest adsorption sites present on the mesopore or external surface [47].

Negligible values of the micropore volume (Table 1, $V_{micro}{}^{b}$) based on the QE-TPDA data found for MWW:Ultrasil and MWW:2Aerosil are consistent not only with the lack of catalytic activity of these materials, but also with the absence of reflections characteristic for MWW framework in the XRD results.

Values of the parameters characterizing porosity are collated in Table 1.

To supplement the evaluation of zeolite content in the mixtures by XRD and the sorption methods, FT-IR spectroscopy was used. The integral intensity of the double band in the range of 500–600 $cm^{-1}$, corresponding to the vibrations of D6R units of the MWW framework (Fig. 6) can be used to quantify the content in a sample [32]. Both silica and zeolite are built of $SiO_4$ tetrahedra, and the internal T–O stretching vibrations are independent of their organization. For this reason, the maximum at 800 $cm^{-1}$, characteristic of stretching symmetric vibrations T–O inside tetrahedra, was used as the normalization factor.

Very low zeolite content in MWW:1Aerosil (20%), MWW:2Aerosil (1%), and MWW:1Ultrasil mixtures (8%) is responsible for the low catalytic activity and is also consistent with the very low microporosity of the samples. This suggests that the attempted deposition of MWW monolayers on solid silicas is not leading to the formation of permanent bonds. Co-precipitation of MWW nanosheets and Ludox produces stable mixtures. However, independently of the amount of Ludox used, the MWW:Ludox ratio is always close to 0.5, although it slightly decreases with an increasing amount of added Ludox (MWW content decreases from 56 to 50 and 43%). Catalytic activity, expressed as $t_{50}$ (time when 50% conversion was reached), was correlated with the calculated content of MWW in prepared mixtures (Fig. 6). It is interesting that for co-precipitated MWW:Ludox mixtures even if the zeolite content is halved, the catalytic activity decreases only by ca. 20% ($t_{50}$ increases from 64–67 to 73–82 min). On the other hand, a physical mixture of MWW_coll with previously precipitated Ludox

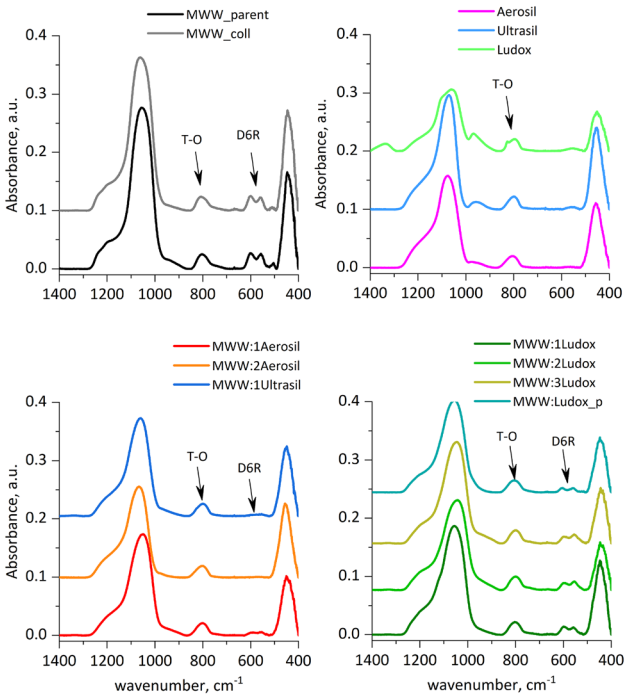


**Fig. 6** ATR spectra in the pseudo-skeletal vibrations region of the studied samples. All spectra are normalized to the same integral intensity of the 800 $cm^{-1}$ maximum (T–O vibrations) and baseline corrected

to the pure MWW, precipitated from the colloidal solution (Fig. 8), with decreased intensity of Si–OH–Al maximum at 3624 $cm^{-1}$ and increased intensity of silanols (3745 $cm^{-1}$) due to the presence of (hydrated) $SiO_2$. In all mixtures, as well as in MWW_coll, the band at 3670 $cm^{-1}$, a characteristic of the partially framework Al, is present [48], but the intensity of this band is rather low and similar for all samples. It should not influence the catalytic activity of the mixtures or block the zeolite channels.

Friedel–Crafts alkylation may be also catalyzed on Lewis acid centers. However, the role of LAS is quite complex. According to a well-established mechanism, LAS may produce carbocation from the alcohol in a two-stage reaction for which formation of carbocation (or alcohol–LAS complex) is the rate determining step [39]. Taking into account that, for the catalysts studied in this paper, the share of LAS does not exceed 21% of all acid sites and that the sample MWW:2Aerosil which contained only LAS (381 µmol/g) did not show any catalytic activity, we attribute their catalytic activity to the Brønsted acid sites located in the 12-MR cups present at the surface of MWW layers.

Based on the determined concentration of active sites it was possible to calculate TOFs as the values representing the average activity of acid sites (Fig. 7c). The highest TOF values were obtained with the MWW:Ludox samples (3.4, 4.1 and $4.8\times\cdot10^{-3}$ $s^{-1}$). Interestingly, the TOF value

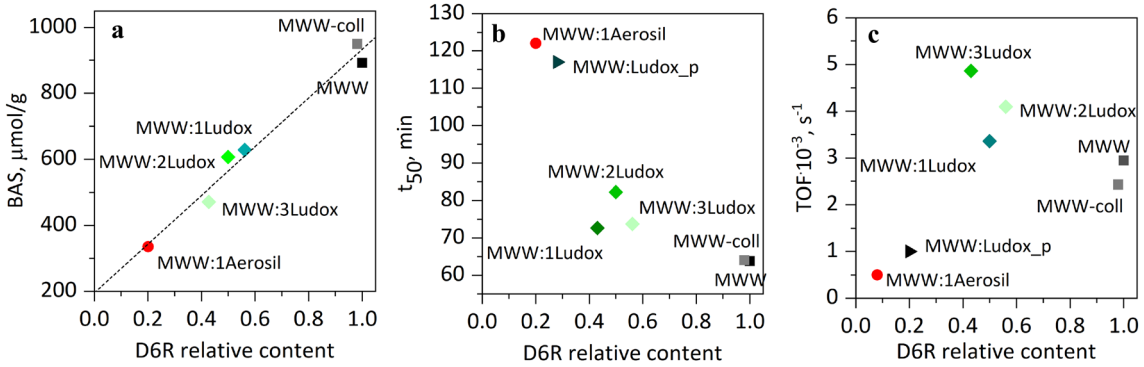


**Fig. 7** **a** Dependence of BAS concentration on the content of MWW zeolite in the MWW:silica mixtures. The dotted line was fitted, $R^2=0.977$, **b** dependence of the catalytic activity ($t_{50}$ values) on the content of MWW zeolite in the MWW:silica mixtures, calculated based on the 500–600 $cm^{-1}$ IR maximum of D6R (double six rings) integrated intensities, and **c** dependence of turnover frequency (TOF) on the content of MWW zeolite in the MWW:silica mixtures

has much lower catalytic activity (MWW content ca. 30%)—$t_{50}$ increase from 64–67 to 122 min, that is, almost doubles.

The zeolite content in the MWW:silica mixtures correlates well with the concentration of BAS, determined by pyridine adsorption (Fig. 6a), suggesting that, since all OH groups are available to pyridine, the layers are not damaged when they are mixed with silica and that silica does not block entrances to the micropores (only their content may be low). The character of OH groups in the mixtures is similar

for MWW:1Aerosil is comparably high, but due to the very low content of the active zeolite phase its overall activity is low with long $t_{50}$ (122 min). The TOF values are comparable to other types of MWW materials such as pillared MWW layers (produced from exfoliated MWW monolayers in solution), where in the best case TOF = $4.61\times\cdot10^{-3}$ $s^{-1}$) [30] and even better than in the case where MWW was mixed with all-silica MFI (TOF = $3.38\times\cdot10^{-3}$ $s^{-1}$) [25].

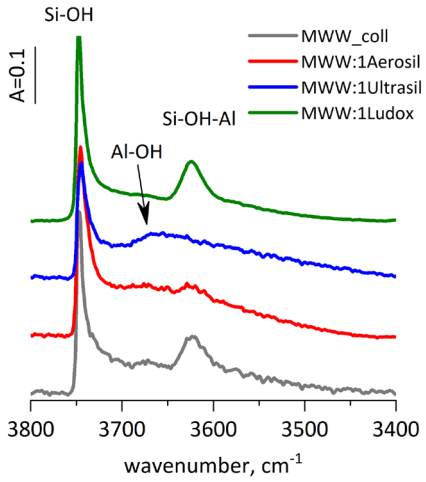


**Fig. 8** FT-IR spectra in the region of OH vibrations for representative samples. Spectra are baseline corrected and vertically shifted

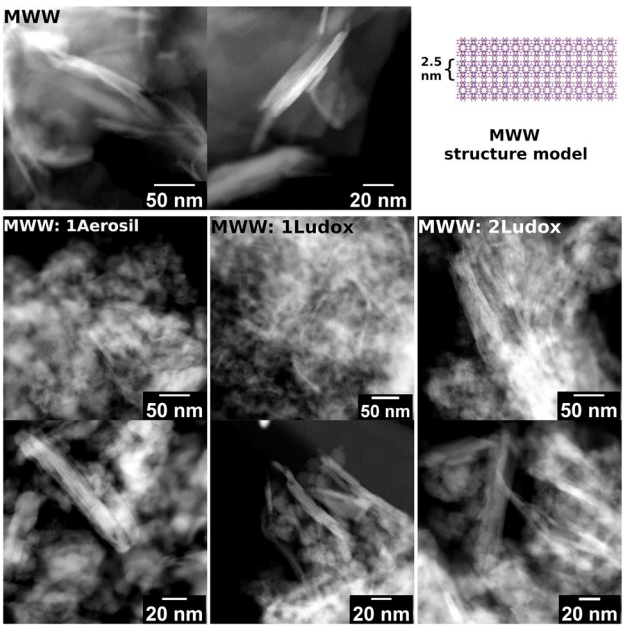


**Fig. 9** STEM images of selected materials: standard MWW, MWW:1Aerosil, MWW:1Ludox, and MWW:2Ludox. In the upper right corner, there is a structural model of MWW with indication of the thickness of a single layer (2.5 nm)

The nature of the Brønsted acid sites did not change when the MWW layers were mixed with silica, which was supported by the positions of the Si–OH–Al maximum at 3624 $cm^{-1}$ in the FT-IR spectra (Fig. 8). At the same time, the catalytic activity of the MWW:Ludox mixtures is comparable (although a bit lower) to that of the pure MWW samples despite the dilution of the active phase of the zeolite. This is accounted for by postulating due to increased accessibility of the acid centers promoted by the added silica. In short, the decreased concentration of active sites was compensated by enhanced access to these reaction centers.

Another valuable information was received from STEM images (Fig. 9), which identify differences in the structure of the three selected materials. For this purpose, only samples showing crystallinity and good catalytic activities were selected: MWW:1Aerosil, MWW:1Ludox, and MWW:2Ludox.

The layers in Aerosil and Ludox silica deposits are well separated, unorganized, scattered, and covered with silica. In the MWW–Ludox materials, some layers stack up close to each other, but not as close as in the MWW_coll, composed of the precipitated MWW layers.

## 4 Conclusions

The results obtained in this study indicate that solids containing MWW layers dispersed on silica support by interaction with a liquid exfoliated MCM-56 zeolite solution, can be promising as catalysts for the transformation of large organic molecules. In particular, composites obtained MWW:silica from colloidal dispersions of MWW monolayers and liquid silica precursors (colloidal silica) exhibit high specific catalytic activity, despite having considerable content of the inactive amorphous silica support. Silica particles in Ludox are dispersed in a liquid, while in the solid sources (Ultrasil and Aerosil) they are agglomerated, hence the effective surface available for interaction with the MWW layers is expected to be lower with them. As a result, the combination of Ludox nanoparticles with MWW monolayers resulted in mixed systems with high dispersion of zeolitic domains. Ethanol is an effective flocculent for zeolite layers by itself, but in the presence of solid silica its efficiency was reduced, indicating its limited effectiveness in the construction of composite catalysts in general. The TOF values ($3.4\times10^{-3}$ to $4.8\times10^{-3}$ $s^{-1}$) calculated for these materials were notably higher than those found for the pristine MWW zeolites ($2.4\times10^{-3}$ to $2.9\times10^{-3}$ $s^{-1}$), which is attributed to the enhanced accessibility of the acid sites. Materials synthesized from solid silica precursors showed low or negligible overall activity which could be attributed to the small content of the zeolitic active phase. Even so, for one such material (MWW:1Aerosil) a notable high TOF ($4.8\times10^{-3}$ $s^{-1}$) was found.

**Acknowledgements** This work was financed with funds from the National Science Centre Poland, Grant No. 2020/37/B/ST5/01258. K.O. has been partly supported by the EU Project POWR.03.02.00-00-I004/16.

**Author contributions** All authors contributed to the study. K.O. - synthesis, modifications and catalytic tests, preparing draft of the

manuscript and figures. G. J and A.K. - porosity characterization (measurements and data interpretation). M.M. and A.L. - electron microscopy imaging (measurements and data interpretation). W.J.R - synthesis and modifications, preparing the final version of the manuscript, B.G. - IR spectroscopy (measurements and data interpretation), preparing the final version of the manuscript and figures, W.M. - porosity characterization (data interpretation), preparing the final version of the manuscript.

## Declarations

**Conflict of interest** The authors declare that they have no conflict of interest.



## References

1. P.J. Landrigan, R. Fuller, N.J.R. Acosta, O. Adeyi, R. Arnold, N. Basu, A.B. Balde, R. Bertollini, S. Bose-O'Reilly, J.I. Boufford, P.N. Breysse, T. Chiles, C. Mahidol, A.M. Coll-Seck, M.L. Cropper, J. Fobil, V. Fuster, M. Greenstone, A. Haines, D. Hanrahan, D. Hunter, M. Khare, A. Krupnick, B. Lanphear, B. Lohani, K. Martin, K.V. Mathiasen, M.A. McTeer, C.J.L. Murray, J.D. Ndahimananjara, F. Perera, J. Potocnik, A.S. Preker, J. Ramesh, J. Rockstrom, C. Salinas, L.D. Samson, K. Sandilya, P.D. Sly, K.R. Smith, A. Steiner, R.B. Stewart, W.A. Suk, O.C.P. van Schayck, G.N. Yadama, K. Yumkella, M. Zhong, The Lancet Commission on Pollution and Health. Lancet **391**, 462–512 (2018)
2. P. Falkowski, R.J. Scholes, E. Boyle, J. Canadell, D. Canfield, J. Elser, N. Gruber, K. Hibbard, P. Hogberg, S. Linder, F.T. Mackenzie, B. Moore, T. Pedersen, Y. Rosenthal, S. Seitzinger, V. Smetacek, W. Steffen, The global carbon cycle: a test of our knowledge of earth as a system. Science **290**, 291–296 (2000)
3. M.R. Chertow, Industrial symbiosis: literature and taxonomy. Annu. Rev. Energy Environ. **25**, 313–337 (2000)
4. Y. Loganathan, M.P.J. Kizhakedathil, A review on microplastics—an indelible ubiquitous pollutant. Biointerface Res. Appl. Chem. **13**(2), 126 (2023)
5. B.L. Chean-Yiing, S.Y. Yusuf, N.R. Jamian, R.M. Kasmani, A.M. Rashid, D. Naidu, E.A. Wikurendra, A.H.Z. Fasya, A review on the effects of flame retardant additives towards the environment and human health. Biointerface Res. Appl. Chem. **12**, 7983–7993 (2022)
6. G.D. Tian, G. Yuan, A. Aleksandrov, T.Z. Zhang, Z.W. Li, A.M. Fathollahi-Fard, M. Ivanov, Recycling of spent lithium-ion batteries: a comprehensive review for identification of main challenges and future research trends. Sustain. Energy Technol. Assess. **53**, 102447 (2022)
7. B. Yilmaz, U. Müller, Catalytic applications of zeolites in chemical industry. Top. Catal. **52**, 888–895 (2009)
8. D. Kerstens, B. Smeyers, J. Van Waeyenberg, Q. Zhang, J. Yu, B.F. Sels, State of the art and perspectives of hierarchical zeolites: practical overview of synthesis methods and use in catalysis. Adv. Mater. **32**, 2004690 (2020)
9. P.T. Anastas, M.M. Kirchhoff, T.C. Williamson, Catalysis as a foundational pillar of green chemistry. Appl. Catal. A **221**, 3–13 (2001)
10. G. Singh, J. Lee, A. Karakoti, R. Bahadur, J.B. Yi, D.Y. Zhao, K. AlBahily, A. Vinu, Emerging trends in porous materials for $CO_{(2)}$ capture and conversion. Chem. Soc. Rev. **49**, 4360–4404 (2020)
11. L.P. Han, S.X. Cai, M. Gao, J. Hasegawa, P.L. Wang, J.P. Zhang, L.Y. Shi, D.S. Zhang, Selective catalytic reduction of $NO_x$ with $NH_3$ by using novel catalysts: state of the art and future prospects. Chem. Rev. **119**, 10916–10976 (2019)
12. Y. Li, L. Li, J.H. Yu, Applications of zeolites in sustainable chemistry. Chem **3**, 928–949 (2017)
13. L. Wu, Y. Li, Z.Y. Fu, B.L. Su, Hierarchically structured porous materials: synthesis strategies and applications in energy storage. Natl Sci. Rev. **7**, 1667–1701 (2020)
14. D. Azizi, F. Ibsaine, J. Dionne, L.C. Pasquier, L. Coudert, J.F. Blais, Microporous and macroporous materials state-of-the-art of the technologies in zeolitization of aluminosilicate bearing residues from mining and metallurgical industries: a comprehensive review. Microporous Mesoporous Mater. **318**, 111029 (2021)
15. S. Mintova, M. Jaber, V. Valtchev, Nanosized microporous crystals: emerging applications. Chem. Soc. Rev. **44**, 7207–7233 (2015)
16. M.C. Silaghi, C. Chizallet, P. Raybaud, Challenges on molecular aspects of dealumination and desilication of zeolites. Microporous Mesoporous Mater. **191**, 82–96 (2014)
17. A. Schwanke, S. Pergher, Lamellar MWW-type zeolites: toward elegant nanoporous materials. Appl. Sci. (Basel) **8**(9), 1636 (2018)
18. W.J. Roth, B. Gil, W. Makowski, B. Marszalek, P. Eliasova, Layer like porous materials with hierarchical structure. Chem. Soc. Rev. **45**, 3400–3438 (2016)
19. P. Wu, J.F. Ruan, L.L. Wang, L.L. Wu, Y. Wang, Y.M. Liu, W.B. Fan, M.Y. He, O. Terasaki, T. Tatsumi, Methodology for synthesizing crystalline metallosilicates with expanded pore windows through molecular alkoxysilylation of zeolitic lamellar precursors. J. Am. Chem. Soc. **130**, 8178–8187 (2008)
20. S. Inagaki, T. Tatsumi, Vapor-phase silylation for the construction of monomeric silica puncheons in the interlayer micropores of Al-MWW layered precursor. Chem. Commun. (2009). https://doi.org/10.1039/B823524D
21. A. Corma, V. Fornes, S.B. Pergher, T.L.M. Maesen, J.G. Buglass, Delaminated zeolite precursors as selective acidic catalysts. Nature **396**, 353–356 (1998)
22. X.Y. Zhang, D.X. Liu, D.D. Xu, S. Asahina, K.A. Cychosz, K.V. Agrawal, Y. Al Wahedi, A. Bhan, S. Al Hashimi, O. Terasaki, M. Thommes, M. Tsapatsis, Synthesis of self-pillared zeolite nanosheets by repetitive branching. Science **336**, 1684–1687 (2012)
23. K. Na, M. Chol, W. Park, Y. Sakamoto, O. Terasakl, R. Ryoo, Pillared MFI zeolite nanosheets of a single-unit-cell thickness. J. Am. Chem. Soc. **132**, 4169–4177 (2010)
24. W.J. Roth, T. Sasaki, K. Wolski, Y. Song, D.-M. Tang, Y. Ebina, R. Ma, J. Grzybek, K. Kałahurska, B. Gil, M. Mazur, S. Zapotoczny, J. Cejka, Liquid dispersions of zeolite monolayers with high catalytic activity prepared by soft-chemical exfoliation. Sci. Adv. **6**, eaay8163 (2020)

25. K. Ogorzaly, B. Gil, M. Mazur, W. Makowski, W.J. Roth, Mixed zeolite hybrids combining the MFI structure with exfoliated MWW monolayers. Microporous Mesoporous Mater. **324**, 111300 (2021)
26. J.N. Coleman, M. Lotya, A. O'Neill, S.D. Bergin, P.J. King, U. Khan, K. Young, A. Gaucher, S. De, R.J. Smith, I.V. Shvets, S.K. Arora, G. Stanton, H.Y. Kim, K. Lee, G.T. Kim, G.S. Duesberg, T. Hallam, J.J. Boland, J.J. Wang, J.F. Donegan, J.C. Grunlan, G. Moriarty, A. Shmeliov, R.J. Nicholls, J.M. Perkins, E.M. Grieveson, K. Theuwissen, D.W. McComb, P.D. Nellist, V. Nicolosi, Two-dimensional nanosheets produced by liquid exfoliation of layered materials. Science **331**, 568–571 (2011)
27. V. Nicolosi, M. Chhowalla, M.G. Kanatzidis, M.S. Strano, J.N. Coleman, Liquid exfoliation of layered materials. Science **340**, 1420 (2013)
28. K. Ogorzały, G. Jajko, K. Wolski, S. Zapotoczny, M. Kubů, W.J. Roth, B. Gil, W. Makowski, Catalytic activity enhancement in pillared zeolites produced from exfoliated MWW monolayers in solution. Catal. Today **390–391**, 272–280 (2021)
29. E. Xing, Y. Shi, W. Xie, F. Zhang, X. Mu, X. Shu, Perspectives on the multi-functions of aniline: cases from the temperature-controlled phase transfer hydrothermal synthesis of MWW zeolites. Microporous Mesoporous Mater. **254**, 201–210 (2017)
30. K. Ogorzaly, A. Wegrzyn, A. Korzeniowska, A. Slawek, A. Kowalczyk, B. Gil, W.J. Roth, W. Makowski, Structure–catalytic properties relationship in Friedel-Crafts alkylation reaction for MCM-36-type zeolites obtained by isopropanol-assisted pillaring. Catalysts **11**(3), 299 (2021)
31. E.H. Xing, Y.C. Shi, W.H. Xie, F.M. Zhang, X.H. Mu, X.T. Shu, Temperature-controlled phase-transfer hydrothermal synthesis of MWW zeolites and their alkylation performances. RSC Adv. **6**, 29707–29717 (2016)
32. B. Gil, W.J. Roth, W. Makowski, B. Marszalek, D. Majda, Z. Olejniczak, P. Michorczyk, Facile evaluation of the crystallization and quality of the transient layered zeolite MCM-56 by infrared spectroscopy. Catal. Today **243**, 39–45 (2015)
33. W. Makowski, Quasi-equilibrated temperature programmed desorption and adsorption: a new method for determination of the isosteric adsorption heat. Thermochim. Acta **454**, 26–32 (2007)
34. W. Makowski, B. Gil, D. Majda, Characterization of acidity and porosity of zeolite catalysts by the equilibrated thermodesorption of *n*-hexane and *n*-nonane. Catal. Lett. **120**, 154–160 (2008)
35. W. Makowski, L. Chmielarz, P. Kuśtrowski, Determination of the pore size distribution of mesoporous silicas by means of quasi-equilibrated thermodesorption of *n*-nonane. Microporous Mesoporous Mater. **120**, 257–262 (2009)
36. Y.C. Shi, E.H. Xing, W.H. Xie, F.M. Zhang, X.H. Mu, X.T. Shu, Shape selectivity of beta and MCM-49 zeolites in liquid-phase alkylation of benzene with ethylene. J. Mol. Catal. A **418**, 86–94 (2016)
37. B. Zhang, Y.J. Ji, Z.D. Wang, Y.M. Liu, H.M. Sun, W.M. Yang, P. Wu, Liquid-phase alkylation of benzene with ethylene over postsynthesized MCM-56 analogues. Appl. Catal. A **443**, 103–110 (2012)
38. F. Zhao, Y. Zhang, S.D. Geng, L.F. Chen, W. Wang, Structure, acid properties and catalysis performance of MCM-22 "Family" zeolites on the alkylation of benzene with propylene. Chem. Eng. Mater. Propert. **II**(549), 283–286 (2012)
39. A. Korzeniowska, J. Grzybek, K. Kałahurska, M. Kubu, W.J. Roth, B. Gil, The structure–catalytic activity relationship for the transient layered zeolite MCM-56 with MWW topology. Catal. Today **345**, 116–124 (2020)
40. V.A. Ostroumova, A.L. Maksimov, MWW-type zeolites: MCM-22, MCM-36, MCM-49, and MCM-56 (a review). Pet. Chem. **59**, 788–801 (2019)
41. W.J. Roth, MCM-22 zeolite family and the delaminated zeolite MCM-56 obtained in one-step synthesis. Stud. Surf. Sci. Catal. **158**, 19–26 (2005)
42. R.H. Archer, J.R. Carpenter, S.J. Hwang, A.W. Burton, C.Y. Chen, S.I. Zones, M.E. Davis, Physicochemical properties and catalytic behavior of the molecular sieve SSZ-70. Chem. Mater. **22**, 2563–2572 (2010)
43. S. Smeets, Z.J. Berkson, D. Xie, S.I. Zones, W. Wan, X. Zou, M.-F. Hsieh, B.F. Chmelka, L.B. McCusker, C. Baerlocher, Well-defined silanols in the structure of the calcined high-silica zeolite SSZ-70: new understanding of a successful catalytic material. J. Am. Chem. Soc. **139**, 16803–16812 (2017)
44. M. Thommes, Physical adsorption characterization of nanoporous materials. Chem. Ing. Tech. **82**, 1059–1073 (2010)
45. M. Thommes, K. Kaneko, A.V. Neimark, J.P. Olivier, F. Rodriguez-Reinoso, J. Rouquerol, K.S.W. Sing, Physisorption of gases, with special reference to the evaluation of surface area and pore size distribution (IUPAC Technical Report). Pure Appl. Chem. **87**, 1051–1069 (2015)
46. K.S.W. Sing, R.T. Williams, Physisorption hysteresis loops and the characterization of nanoporous materials. Adsorpt. Sci. Technol. **22**, 773–782 (2004)
47. W. Makowski, P. Kuśtrowski, Probing pore structure of microporous and mesoporous molecular sieves by quasi-equilibrated temperature programmed desorption and adsorption of *n*-nonane. Microporous Mesoporous Mater. **102**, 283–289 (2007)
48. A. Janin, M. Maache, J.C. Lavalley, J.F. Joly, F. Raatz, N. Szydlowski, FT IR study of the silanol groups in dealuminated HY zeolites: nature of the extra framework debris. Zeolites **11**, 391–396 (1991)